

Analytical Synchronization Analysis of Line-Start Permanent Magnet Synchronous Motors

Abdoulkadri Chama, Albert J. Sorgdrager, and Rong-Jie Wang*

Abstract—A main challenge in designing line-start permanent magnet synchronous motors is synchronization analysis and determination. The transient time-step finite element simulations are often required in the design process, which is computationally expensive. An attractive alternative is to use an analytical synchronization model, which is time efficient and thus viable to be included in an optimization procedure. In this paper, two variants of the energy-based analytical synchronization model are proposed. Their viability and performance are compared with those of the existing analytical method and validated by transient finite element simulations. It is shown that the proposed methods have a better resolution and accuracy in determining the synchronization status of line-start permanent magnet motors.

1. INTRODUCTION

Line-start permanent magnet synchronous motors (LS-PMSMs) are ideally suitable for fixed speed industrial applications such as fans, compressors and pumps drives [1]. Self-starting capability is a key advantage, but also a design challenge for LS-PMSMs [1, 2]. When designing an LS-PMSM, both steady-state and transient operations need to be considered. Various design strategies have been proposed in the past [2, 3]. One common design approach is to first optimize the steady-state performance, and then verify the synchronization capability of the design by using transient finite element (FE) simulations [4–6]. Some recent works use different optimization methods (e.g., the Taguchi method [7], Genetic Algorithm (GA) [8] and Particle Swarm Optimization (PSO) [9]) in a multi-objective setup coupled with transient performance constraints in an attempt to realize a balanced design with limited or without use of transient FE analysis.

Since transient FE simulations are time consuming, they become prohibitively expensive from computational perspective to incorporate them into a full optimization procedure. As an alternative, the use of an analytical synchronization model has been proposed by researchers such as Honsinger [10], Miller [11], Rahman et al. [12–14], and Soulard and Nee [15]. These analytical models are very efficient and can be readily implemented into a design optimization routine to minimize the use of costly transient time-step FE simulations [16, 17]. Among them, the energy based synchronization model has been widely accepted [13, 14]. In this paper, two variants of the energy based synchronization approach are proposed. Their viability and performance are compared with those of the existing analytical method and validated by transient FE simulations.

2. ANALYTICAL SYNCHRONIZATION MODELS

An LS-PMSM, as shown in Figure 1(a), has a hybrid rotor containing both cage winding and permanent magnets (PMs). The transient state of an LS-PMSM is rather complex as the behavior of the motor is

Received 3 May 2016, Accepted 7 June 2016, Scheduled 23 June 2016

* Corresponding author: Rong-Jie Wang (rwang@sun.ac.za).

The authors are with the Department of Electrical and Electronic Engineering, Stellenbosch University, Private Bag X1, Matieland 7602, South Africa.

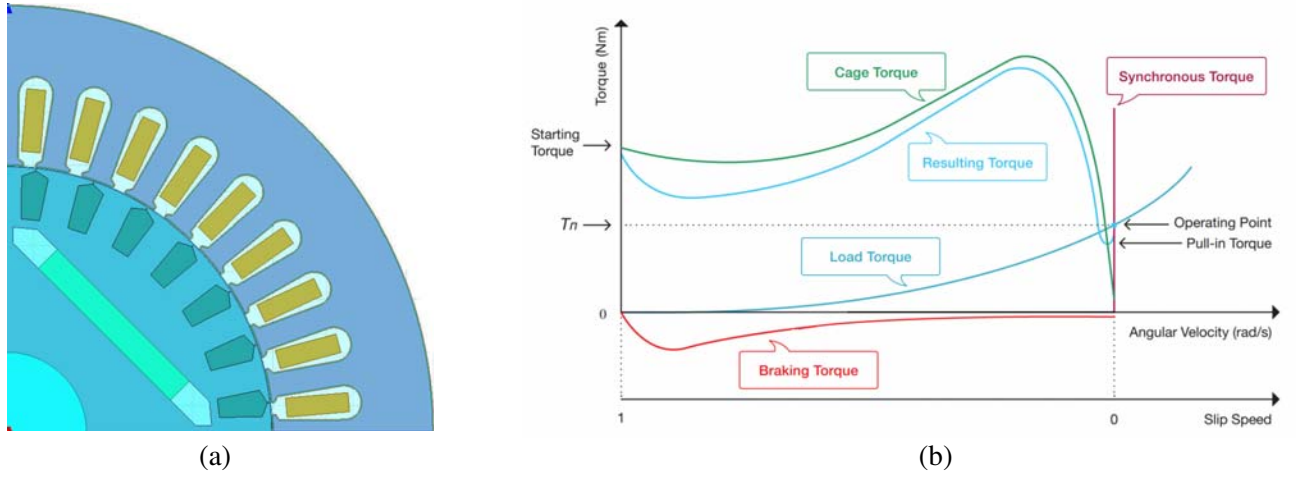


Figure 1. (a) The cross-section layout and (b) torque components of an LS-PMSM.

affected by several torque components as illustrated in Figure 1(b), where cage, braking and synchronous torques are represented by T_c , T_b and T_s hereinafter. According to [10, 14, 18], these torque components can be expressed as functions of the slip s and load angle δ in radians as follows:

$$T_b(s) = -\frac{mpE_0^2 R_1}{2\pi f} \cdot \frac{[R_1^2 + (1-s)^2 X_q^2] (1-s)}{[R_1^2 + (1-s)^2 X_q X_d]^2} \quad (1)$$

$$T_c(s) = \frac{mp}{2\pi f} \cdot \frac{s R_2' V_{ph}^2}{(s R_1 + c_1 R_2')^2 + s^2 (X_1 + c_1 X_2')^2} \quad (2)$$

$$T_s(\delta) = T_{s_0} + T_{s_1} \sin \delta + T_{s_2} \sin 2\delta + T_{s_3} \cos \delta + T_{s_4} \cos 2\delta \quad (3)$$

where

$$X_d = X_1 + X_{ad}, \quad X_q = X_1 + X_{aq}, \quad c_1 = 1 + \frac{X_1}{X_m} \quad (4)$$

$$X_m = \frac{2 \cdot X_{ad} X_{aq}}{X_{ad} + X_{aq}} \quad (5)$$

The components of T_s are described by Eqs. (A1)–(A5). A list of symbols used in these equations is given in A.2.

2.1. Energy-Based Model: A New Algorithm

From Eqs. (1)–(3), the average and instantaneous torques can be defined as follows:

$$T_a(s) = T_c(s) + T_b(s) \quad \text{and} \quad T_i(s, \delta) = T_s(\delta) + T_a(s) - T_l(s)$$

with $T_l(s) = T_{\text{rated}}(1-s)^2$ being the load torque; T_{rated} is the rated torque of the motor at synchronous speed. The instantaneous torque T_i follows the equation of motion in the $s - \delta$ plane, i.e.,

$$-\frac{J\omega_s^2}{p} \cdot s \frac{ds}{d\delta} = T_i(s, \delta) \quad (6a)$$

Equation (6a) is a nonlinear partial differential equation (PDE) and can be solved by the implicit Runge-Kutta-Fehlberg method. To implement the method, Eq. (6a) can be first written in the form:

$$\frac{ds}{d\delta} = -\frac{p}{J\omega_s^2 s} T_i(s, \delta) = f(s, \delta) \quad (6b)$$

Starting with an initial condition $s_0 = s(0) = 1$, the five-stage coefficient $K_j, j = 1, \dots, 5$ are evaluated at each iteration:

$$\begin{aligned}
 K_1 &= hf(s_i, \delta_i) \\
 K_2 &= hf(s_i + \gamma_{11}K_1, \delta_i + \alpha_1h) \\
 K_3 &= hf(s_i + \gamma_{21}K_1 + \gamma_{22}K_2, \delta_i + \alpha_2h) \\
 K_4 &= hf(s_i + \gamma_{31}K_1 + \gamma_{32}K_2 + \gamma_{33}K_3, \delta_i + \alpha_3h) \\
 K_5 &= hf(s_i + \gamma_{41}K_1 + \gamma_{42}K_2 + \gamma_{43}K_3 + \gamma_{44}K_4, \delta_i + \alpha_4h)
 \end{aligned}
 \tag{7a}$$

where h is the step size, and γ_{jn} and α_j are the coefficients of Butcher table for the Fehlberg’s 4–5 order method [19]. Next the 4th and 5th order Runge-Kutta approximate solutions y_{i+1} and z_{i+1} of problem (6b) are computed:

$$y_{i+1} = y_i + b_1K_1 + b_3K_3 + b_4K_4 + b_5K_5 \tag{7b}$$

$$z_{i+1} = y_i + d_1K_1 + d_3K_3 + d_4K_4 + d_5K_5, \tag{7c}$$

respectively. The coefficients b_i and d_i are given in [19]. The local discretization error is then expressed as:

$$\tau = \frac{|y_{i+1} - z_{i+1}|}{h_{i+1}} \tag{8}$$

If τ is smaller than the set tolerance in the implementation, then the approximation is accepted; else a new step size

$$h_{\text{new}} = h \cdot 0.84 \cdot \left(\frac{\text{tolerance}}{|z_{i+1} - y_{i+1}|} \right)^{\frac{1}{4}} \tag{9}$$

is chosen for a better convergence. The program terminates if the value $s = 0$ is found within a tolerance less than 10^{-10} .

Figure 2(a) shows the slip as a function of the load angle obtained by the numerical implementation of the Runge-Kutta-Fehlberg method. Figure 2(b) compares this implementation with the approximation of the synchronization region proposed in [14]. Clearly, there exists a good agreement between the two approaches. However, to the contrary of [14], where the proof and error estimate have been omitted, the proposed approximation is well known to have at least a 4th order of convergence. Choosing the mesh size h to be small enough would allow us to reach the critical synchronization state with a very small relative error.

One of the advantages of the direct resolution of the PDE in Eq. (6) is that it allows in certain context to easily recognize the synchronization capability of the machine without deeper treatment of the problem. Figures 2(c) and 3(a) show clear indication of non-synchronized machine, whereas Figure 3(b) shows that the machine does synchronize to operate at rated conditions of the machine.

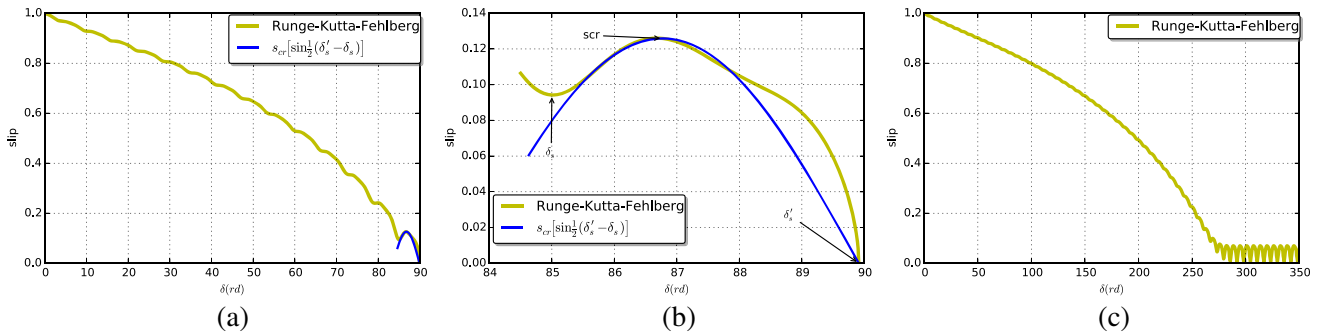


Figure 2. Slip as a function of load angle of (a) a synchronized machine; (b) the critical synchronized region of (a); (c) a non-synchronized machine.

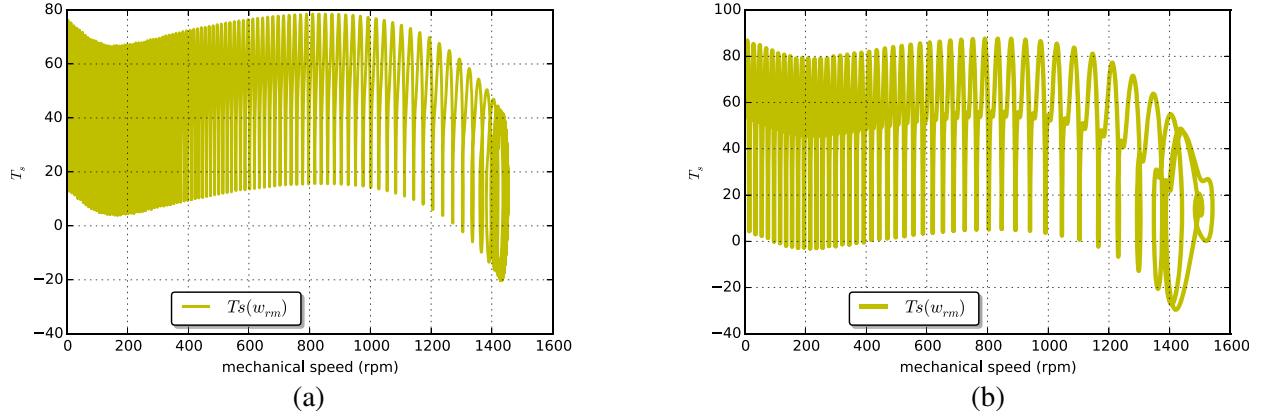


Figure 3. Instantaneous torque of (a) a non-synchronized machine; (b) a synchronized machine.

2.1.1. Synchronization Conditions

The critical synchronization state of the machine is determined within the domain $[\delta_s, \delta'_s]$ [18], which is depicted in Figure 2(b). The necessary kinetic energy E_k to pull the motor into synchronization is evaluated from the critical slip $s = s_{scr}$ to zero slip, $s = 0$:

$$E_k = \int_{s_{scr}}^0 -\frac{1}{p} J \omega_s^2 s \, ds = \frac{1}{2p} J \omega_s^2 s_{scr}^2 \quad (10a)$$

The synchronization energy from point δ_{scr} to δ'_s is

$$E_{syn} = \int_{\delta_{scr}}^{\delta'_s} T_i(s(\delta), \delta) \, d\delta, \quad (10b)$$

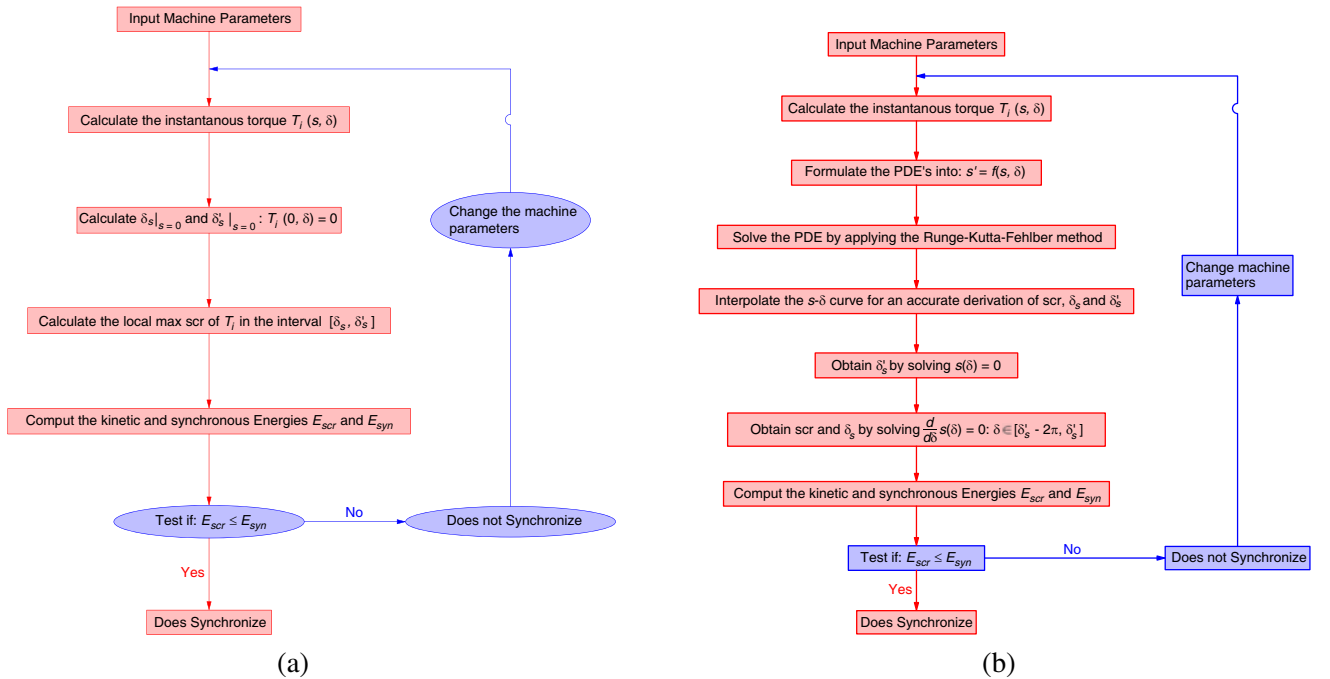


Figure 4. Flowchart describing the implementation of synchronization criteria using (a) simplified method [14]; (b) the proposed method.

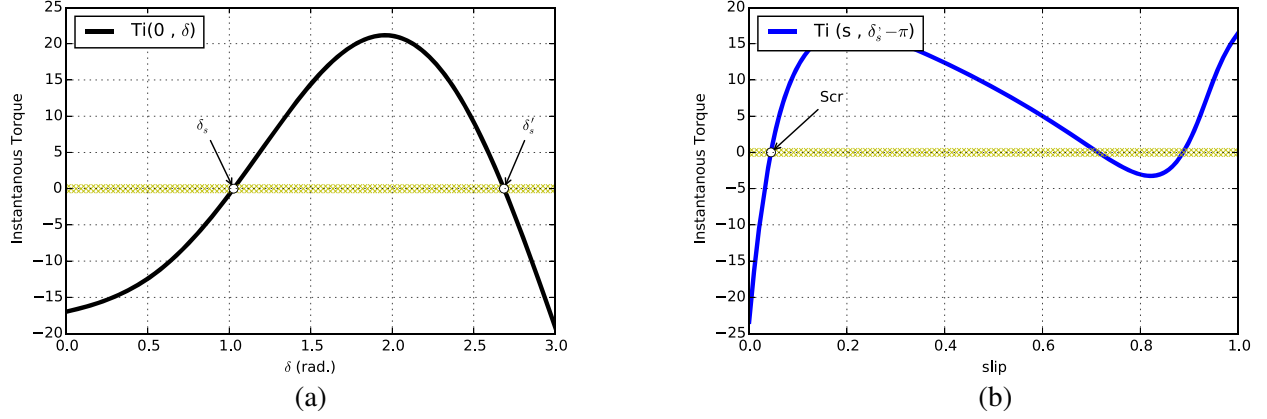


Figure 5. (a) Finding the load angle δ'_s . (b) Finding the critical slip s_{cr} .

where δ_{scr} is the x -axis component of the critical point s_{cr} .

The machine synchronizes under the situation when: $E_{scr} \leq E_{sym}$; otherwise, it does not synchronize. Flowcharts describing the implementation of synchronization criteria by using the simplified method as discussed in [14] and the proposed method in this paper are given in Figure 4. To evaluate the integrals in Eqs. (10a) and (10b), δ'_s needs to be found by solving the equation $T_i(0, \delta) = 0$ as illustrated in Figure 5(a). To obtain the critical slip the equation $T_i(s, \delta'_s - \pi) = 0$ has to be solved (see Figure 5(b)). Note that s_{cr} is the local maximum of the s - δ function nearest to the origin ($s = 0$) and δ'_s the second x -intercept of the curve of T_i .

2.1.2. Issues with Trigonometrical Approximation

The approximation of the synchronization region by a trigonometrical function that strictly depend on δ'_s is often used in literature [11–15]. Although this approximation can simplify the synchronization calculation, it also compromises the accuracy of the synchronization model. Furthermore, there may be isolated cases in a design optimization process where equation $T_i(0, \delta) = 0$ has no solution, and δ'_s cannot be found. This would inevitably lead to undesired disruption or premature termination of an optimization process. The proposed algorithm can address the above issues as it extracts the synchronization region via the resolution of the PDEs in Eq. (6b) and derives δ'_s from the s - δ curve.

2.2. Time Domain Synchronization Model

An alternative way of analyzing synchronization is to use a transient variant formulation of problem in Eq. (6b), which is the problem of finding both the rotor angle $\theta(t)$ and slip $s(t)$ such as

$$J \frac{\partial \Omega}{\partial t} = T_i(s, \theta) \tag{11a}$$

$$-\frac{1}{p} J \omega_s^2 s \frac{\partial s}{\partial \theta} = T_i(s, \theta), \tag{11b}$$

where $\Omega = \frac{\omega_s(1-s)}{p}$, see [18] for more details. Substituting Ω by its expression and $\frac{\partial s}{\partial \theta}$ by $\frac{\partial s}{\partial t} \frac{\partial t}{\partial \theta}$ and using some basic algebraic transformation of system in Eq. (11), the following initial boundary value problem can be derived:

$$\frac{\partial s}{\partial t} = -\frac{p}{J \omega_s} T_i(s, \theta) \tag{12a}$$

$$\frac{\partial \theta}{\partial t} = s \omega_s \tag{12b}$$

To apply the method discussed in Section 2.1, it is handy to transform the system in Eq. (11) into the following standard first-order PDEs:

$$\dot{\mathbf{Y}} = \mathbf{F}(s, \theta), \tag{13}$$

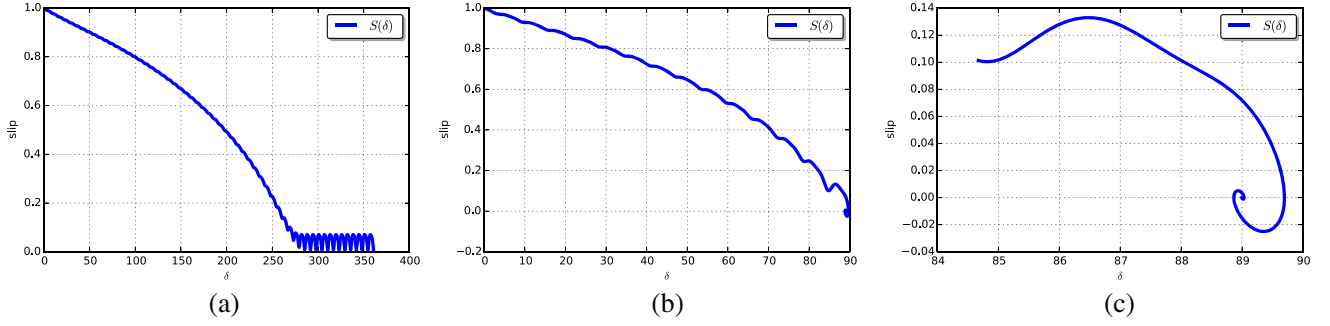


Figure 6. Slip as a function of load angle of (a) a non-synchronized machine; (b) a synchronized machine; (c) the critical synchronized region of (b).

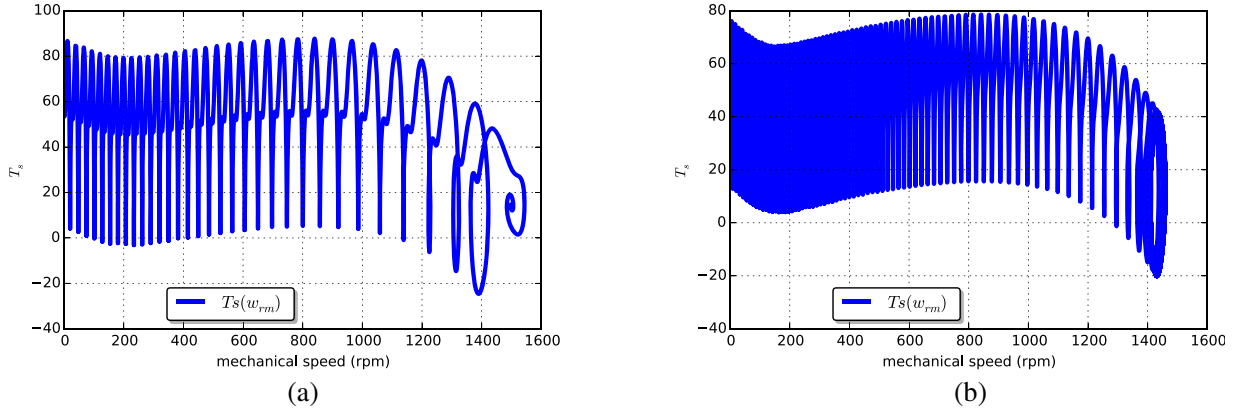


Figure 7. Torque vs. speed of (a) a synchronized machine; (b) a non-synchronized machine.

where $\dot{\mathbf{Y}} = \left[\frac{\partial s}{\partial t}, \frac{\partial \theta}{\partial t} \right]^T$, which can also be solved by any implicit nonlinear time dependent algorithm. Examples of numerical output obtained from the solution of system of Equation (11) are depicted in Figures 6–7.

It should be noted that the synchronization region as shown in Figure 6(c) cannot be obtained from numerical resolution of Equation (6a) because at $s = 0$ the right hand side of Equation (6b) becomes undermined due to the division by zero; whereas Equations (12a) and (12b) are parametrically well posed at $s = 0$.

2.2.1. Synchronization Conditions

With the time domain approach, the speed versus time characteristics obtained from the solution of system in Eq. (12) can be used to study the synchronization capability of the LS-PMSM. The following simple rules can be applied:

- an LS-PMSM is considered as synchronized when the mean value of the speed and its first-order derivative at the last portion of the time interval correspond to synchronous speed and zero respectively;
- an LS-PMSM is considered as not synchronized when its rotational speed oscillates about a mean value below synchronous speed.

Figure 8 displays the numerical solutions obtained from the proposed approach for both synchronized and non-synchronized cases.

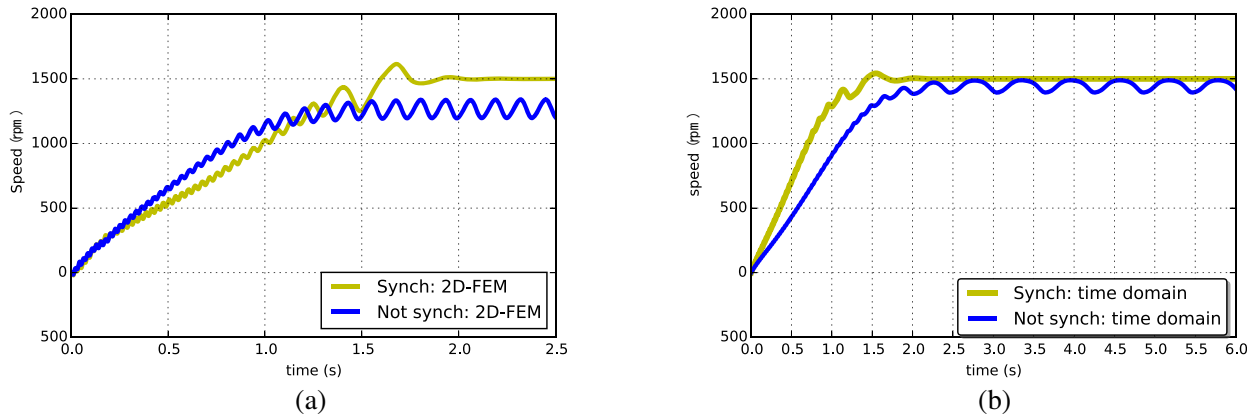


Figure 8. Design 1 in blue (dark color if in gray scale) and design 2 in yellow (light color if in gray scale). (a) Finite element simulation; (b) Time domain simulation.

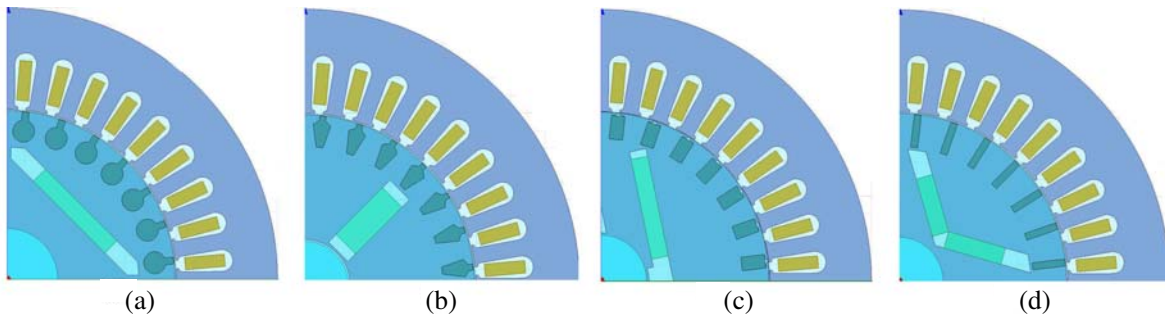


Figure 9. Rotor topologies used to generate candidate designs: (a) radial flux, (b) spoke-type, (c) asymmetric flux, (d) V-type.

3. VERIFICATION OF SYNCHRONIZATION MODEL

In this section, the original synchronization approach (as discussed in [14]) and two proposed variants are applied to a number of different LS-PMSM designs. The results are compared with and validated by FE transient time-step simulation. The basic specifications for all the designs are given in Table 1. In addition, the rotor diameter, stack length and stator slot of all the designs are identical. The differences among these designs are mainly in PM array topologies and rotor slot shapes as illustrated in Figure 9.

The key parameters of the 13 candidate designs are summarized in Table 2. In transient FE time-

Table 1. Machine and load specifications.

Specification	Value
Rated output power, kW	2.2
Rated voltage (line-to-line), V	525
Rated speed, rpm	1500
Rated torque, Nm	14
Frame size	100 L
Load type	Fan
Moment of inertia of the load, kgm ²	0.15
Moment of inertia of the rotor, kgm ²	0.009
Steady-state performance	IE4

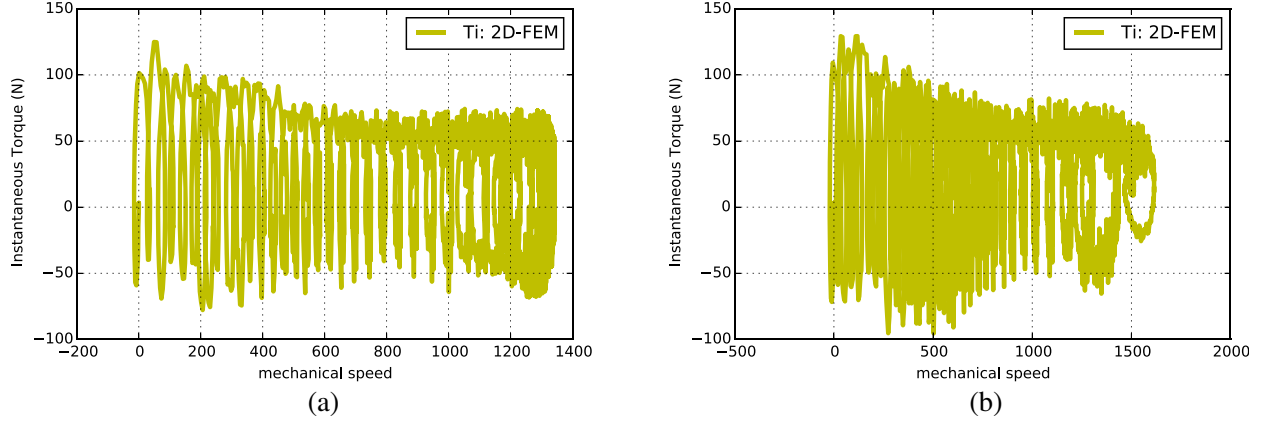


Figure 10. Torque vs speed characteristics obtained from FE for (a) design 1; (b) design 2.

Table 2. Key parameters of the candidate designs.

Design ID	Topology	E_0 (V)	X_{ad} (Ω)	X_{aq} (Ω)	R_1 (Ω)	R'_2 (Ω)	X_1 (Ω)	X'_2 (Ω)
1	Radial	171.20	33.25	99.53	6.63	3.99	3.07	1.80
2	Radial	171.20	33.25	99.53	6.63	2.1	3.07	1.80
3	Asymmetric	232.40	50.08	107.21	6.64	4.11	4.29	1.52
4	Asymmetric	218.36	51.03	107.55	9.91	4.11	4.63	1.52
5	Asymmetric	247.86	51.53	159.32	9.92	2.35	4.22	1.45
6	Asymmetric	241.26	55.22	153.49	7.61	3.22	4.19	2.43
7	Spoke	224.94	37.11	99.72	3.69	2.45	3.06	1.98
8	Spoke	189.60	37.70	101.37	8.42	2.74	3.96	1.85
9	Spoke	227.41	39.07	106.88	8.42	2.85	3.95	2.64
10	V-type	233.03	35.99	172.59	9.66	1.97	6.06	0.832
11	V-type	166.92	37.14	164.94	9.30	3.35	5.61	1.56
12	V-type	187.65	33.63	99.75	8.42	2.89	3.92	2.06
13	V-type	181.16	28.32	101.37	8.43	2.47	3.92	1.63

step simulations, the load equation is defined as $T_l = 14[1 - (157.08 - \omega_r)/157.08]^2$ with ω_r referring to the rotors angular velocity in rad/s. The moment of inertia of the load (J_l) was set at 0.15 kgm^2 , and a time-step of 1 ms was used in the analysis. Using the results from the simulations, both speed-time and instantaneous torque-speed characteristics can be obtained for each candidate design. Figure 10 displays the instantaneous torque versus speed graphs for the two cases (designs 1 and 2). They show the same synchronization states as those of Figure 3 obtained using the proposed analytical approaches. Since the analytical methods use the steady-state parameters of a machine and neglect non-linearity in the calculation, the obtained torque speed curves are somewhat different from FE results. However, the main purpose of the analytical models is to perform fast evaluation of the synchronization states in the critical slip region, where the machine's parameters are much closer to the steady-state ones.

The synchronization states of each design determined by using different analytical models are presented in Table 3. For validation purpose, the transient FE simulation results are used as the reference. For the original energy-based method and its direct PDE resolution variant, the synchronization criterion is $E_{scr} \leq E_{syn}$, whereas for 2D FE and time domain approach, the synchronization state is determined by comparing the average speed with the synchronous speed. It can be seen that all three analytical models correlate reasonably well with the FE results. The proposed direct PDE method obtained a 100% match with FE results while the proposed time domain method and the original approach failed to match in 3 and 4 cases (shown in shaded cells of Table 3), respectively.

Table 3. Synchronization state of candidate designs determined by different analytical models.

Design ID	Original	2D FEM	Direct PDE	Time Domain
1	✗	✗	✗	✗
2	✓	✓	✓	✓
3	✗	✓	✓	✗
4	✗	✗	✗	✗
5	✗	✗	✗	✗
6	✗	✓	✓	✗
7	✓	✓	✓	✓
8	✓	✓	✓	✗
9	✓	✗	✗	✗
10	✓	✗	✗	✗
11	✗	✗	✗	✗
12	✗	✗	✗	✗
13	✗	✗	✗	✗

4. CONCLUSION

In this paper, two variants of the energy based synchronization approach, which uses an implicit nonlinear solver to determine the s - δ plane function and the speed versus time function, are proposed. Despite the simplicity of the algorithm, it provides highly accurate result with a large order of convergence. Indeed even the most popular numerical solvers such as the finite element method can rarely provide a second order of convergence, whereas the algorithm used in our case has fourth order of convergence.

The viability and performance of the new analytical approaches are compared with those of the existing analytical method and validated by transient FE simulations. It is shown that the proposed methods (especially the direct PDE resolution variant) have a better resolution and accuracy in determining the synchronization status of LS-PMSMs than the existing method. Therefore, they are well suited for synchronization analysis for the design optimization of LS-PMSMs.

ACKNOWLEDGMENT

This work was supported in part by Subcommittee B Post-Doctoral Fellowship, Stellenbosch University, and in part by SASOL University Collaboration Initiatives, all of South Africa.

APPENDIX A.

A.1. List of Torque Equations

$$T_{s_0} = \frac{mpR_1X_q}{2\pi f (R_1^2 + X_dX_q)^2} \left[(X_d - X_q) \left(\frac{V_{ph}^2}{2} - 1 + E_0^2 \right) - E_0^2 \left(\frac{R_1^2}{X_q} + X_d \right) \right]; \quad (A1)$$

$$T_{s_1} = \frac{mpE_0V_{ph}}{4\pi f (R_1^2 + X_dX_q)^2} [(X_d - X_q) (R_1^2 - X_dX_q) + (R_1^2 + X_dX_q) X_d]; \quad (A2)$$

$$T_{s_2} = \frac{mpV_{ph}^2}{8\pi f (R_1^2 + X_dX_q)^2} [(X_d - X_q) (X_qX_d - R_1^2)]; \quad (A3)$$

$$T_{s_3} = \frac{mpE_0V_{ph}R_1}{4\pi f (R_1^2 + X_dX_q)^2} [(R_1^2 + X_dX_q) - 2X_q(X_d - X_q)]; \quad (A4)$$

$$T_{s4} = \frac{mpV_{ph}^2 R_1}{8\pi f (R_1^2 + X_d X_q)^2} [(X_d - X_q)(X_d + X_q)] \quad (A5)$$

A.2. List of Symbols

Symbols	Definition	Symbols	Definition
c_1	T_c correction factor	E_o	Back-EMF (V)
E_k	Kinetic energy (J)	E_{syn}	Synchronization energy (J)
E_{scr}	Critical synchronization energy (J)	f	Frequency (Hz)
h	Step/Mesh size	J	Moment of inertia (kgm ²)
J_s	Moment of inertia of system (kgm ²)	l (subscript)	Load
m	Stator phases	p	Pole pairs
R_1	Stator resistance (Ω)	R'_2	Rotor resistance referred (Ω)
r (subscript)	Rotor	s (subscript)	Synchronous/System
s	Slip	s_{cr}	Critical slip
T_a	Average torque (Nm)	T_b	Magnetic braking torque (Nm)
T_c	Cage torque (Nm)	T_i	Instantaneous torque (Nm)
T_s	Synchronous torque (Nm)	X_1	Stator leakage reactance (Ω)
X'_2	Rotor leakage reactance referred (Ω)	X_d/X_q	d-q reactances (Ω)
X_{ad}/X_{aq}	d-q armature reaction reactances (Ω)	V_{ph}	rms phase voltage (V)
δ	Load angle (rad)	δ_s	Synchronous load angle (rad)
δ'_{scr}	Critical load angle (rad)	Ω	Motor speed (rad/s)
ω_s	Electrical synchronous speed (rad/s)	scr (subscript)	Critical

REFERENCES

1. Isfahani, A. H. and S. Vaez-Zadeh, "Line start permanent magnet synchronous motors: Challenges and opportunities," *Energy*, Vol. 34, No. 11, 1755–1763, November 2009.
2. Marčič, T., "A short review of energy-efficient line-start motor design," *Przeglad Elektrotechniczny*, Vol. 87, No. 3, 119–122, 2011.
3. Ugale, R. T., B. N. Chaudhari, and A. Pramanik, "Overview of research evolution in the field of line start permanent magnet synchronous motors," *IET Electr. Power Appl.*, Vol. 8, No. 4, 141–154, April 2014.
4. Fei, W., P. C. K. Luk, J. Ma, J. X. Shen, and G. Yang, "A high-performance line-start permanent magnet synchronous motor amended from a small industrial three-phase induction motor," *IEEE Transactions on Magnetics*, Vol. 45, No. 10, 4724–4727, October 2009.
5. Jazdzynski, W. and M. Bajek, "Modeling and bi-criterial optimization of a line start permanent magnet synchronous machine to find an IE4 class high efficiency motor," *Proceedings of International Conference on Electrical Machines*, Rome, September 6–8, 2010, doi: 10.1109/ICELMACH.2010.5607751.
6. Ruan, T., H. Pan, and Y. Xia, "Design and analysis of two different line-start PM synchronous motors," *2nd International Conference on Artificial Intelligence, Management Science and Electronic Commerce (AIMSEC)*, 3843–3847, China, 2011.
7. Kim, W. H., et al., "A study on the optimal rotor design of LSPM considering the starting torque and efficiency," *IEEE Transactions on Magnetics*, Vol. 45, No. 3, 1808–1811, March 2009.
8. Shamlou, S. and M. Mirsalim, "Design, optimisation, analysis and experimental verification of a new line-start permanent magnet synchronous shaded-pole motor," *IET Electric Power Applications*, Vol. 7, No. 1, 16–26, January 2013.
9. Knypiński, L., L. Nowak, and C. Jedryczka, "Optimization of the rotor geometry of the line-start permanent magnet synchronous motor by the use of particle swarm optimization," *COMPEL*

- *The International Journal for Computation and Mathematics in Electrical and Electronic Engineering*, Vol. 34, No. 3, 882–892, 2015.
10. Honsinger, V. B., “Permanent magnet machines: Asynchronous operation,” *IEEE Trans. on Power Apparatus and Systems*, Vol. 99, No. 4, 1503–1509, July 1980.
 11. Miller, T. J. E., “Synchronization of line-start permanent magnet AC motors,” *IEEE Trans. on Power Apparatus and Systems*, Vol. 103, No. 7, 1822–1828, July 1984.
 12. Rahman, M. A., A. M. Osheiba, and T. S. Radwan, “Synchronization process of line-start permanent magnet synchronous motors,” *Electric Machines and Power Systems*, Vol. 24, No. 6, 577–592, 1997.
 13. Isfahani, A. H., S. Vaez-Zadeh, and M. A. Rahman, “Evaluation of synchronization capability in line start permanent magnet synchronous motors,” *IEEE International Electric Machines and Drives Conference (IEMDC)*, 1346–1350, May 15–18, 2011.
 14. Rabbi, S. F. and M. A. Rahman, “Critical criteria for successful synchronization of line-start IPM motors,” *IEEE Journal of Emerging and Selected Topics in Power Electronics*, Vol. 2, No. 2, 348–358, June 2014.
 15. Soulard, J. and H. P. Nee, “Study of the synchronization of line-start permanent magnet synchronous motors,” *IEEE Industry Applications Conference*, Vol. 1, 424–431, 2000.
 16. Stoia, D., M. Cernat, A. A. Jimoh, and D. V. Nicolae, “Analytical design and analysis of line-start permanent magnet synchronous motors,” *IEEE AFRICON*, 1–7, Nairobi, 2009, doi: 10.1109/AFRCON.2009.5308177
 17. Kurihara, K. and M. A. Rahman, “High-efficiency line-start interior permanent-magnet synchronous motors,” *IEEE Transactions on Industry Applications*, Vol. 40, No. 3, 789–796, May–June 2004.
 18. Tang, R. Y., *Modern Permanent Magnet Machines: Theory and Design*, China Machine Press, Beijing, December 1997.
 19. Dormand, J. R., *Numerical Methods for Differential Equations: A Computational Approach*, CRC Press, February 1996.